JNS

CLINICAL ARTICLE

J Neurosurg 136:358–368, 2022

Memory recovery in relation to default mode network impairment and neurite density during brain tumor treatment

***Rafael Romero-Garcia, PhD,[1] John Suckling, PhD,[1–3] Mallory Owen, MBChB,[1] Moataz Assem, MBBCh, PhD,[4] Rohitashwa Sinha, BMBS, FRCS,[5] Pedro Coelho,[6] Emma Woodberry, PhD,[7] Stephen J. Price, MBBS, PhD,[5] Amos Burke, MD, PhD,[8] Thomas Santarius, MD, PhD,[5,9] Yaara Erez, PhD,[4] and Michael G. Hart, MBChB, PhD[5]**

[1]Department of Psychiatry, University of Cambridge; [2]Behavioural and Clinical Neuroscience Institute, University of Cambridge; [3]Cambridge and Peterborough NHS Foundation Trust, Cambridge; [4]MRC Cognition and Brain Sciences Unit, University of Cambridge; [5]Department of Neurosurgery, Addenbrooke's Hospital, Cambridge; [6]Neurophys Limited, Cambridge; [7]Department of Neuropsychology, Cambridge University Hospitals NHS Foundation Trust, Cambridge; [8]Department of Paediatric Haematology, Oncology, and Palliative Care, Addenbrooke's Hospital, Cambridge; and [9]Department of Physiology, Development, and Neuroscience, University of Cambridge, Cambridgeshire, United Kingdom

OBJECTIVE The aim of this study was to test brain tumor interactions with brain networks, thereby identifying protective features and risk factors for memory recovery after resection.

METHODS Seventeen patients with diffuse nonenhancing glioma (ages 22–56 years) underwent longitudinal MRI before and after surgery, and during a 12-month recovery period (47 MRI scans in total after exclusion). After each scanning session, a battery of memory tests was performed using a tablet-based screening tool, including free verbal memory, overall verbal memory, episodic memory, orientation, forward digit span, and backward digit span. Using structural MRI and neurite orientation dispersion and density imaging (NODDI) derived from diffusion-weighted images, the authors estimated lesion overlap and neurite density, respectively, with brain networks derived from normative data in healthy participants (somatomotor, dorsal attention, ventral attention, frontoparietal, and default mode network [DMN]). Linear mixed-effect models (LMMs) that regressed out the effect of age, gender, tumor grade, type of treatment, total lesion volume, and total neurite density were used to test the potential longitudinal associations between imaging markers and memory recovery.

RESULTS Memory recovery was not significantly associated with either the tumor location based on traditional lobe classification or the type of treatment received by patients (i.e., surgery alone or surgery with adjuvant chemoradiotherapy). Nonlocal effects of tumors were evident on neurite density, which was reduced not only within the tumor but also beyond the tumor boundary. In contrast, high preoperative neurite density outside the tumor but within the DMN was associated with better memory recovery (LMM, p value after false discovery rate correction [P_{fdr}] < 10^{-3}). Furthermore, postoperative and follow-up neurite density within the DMN and frontoparietal network were also associated with memory recovery (LMM, P_{fdr} = 0.014 and P_{fdr} = 0.001, respectively). Preoperative tumor and postoperative lesion overlap with the DMN showed a significant negative association with memory recovery (LMM, P_{fdr} = 0.002 and P_{fdr} < 10^{-4}, respectively).

CONCLUSIONS Imaging biomarkers of cognitive recovery and decline can be identified using NODDI and resting-state networks. Brain tumors and their corresponding treatment affecting brain networks that are fundamental for memory functioning such as the DMN can have a major impact on patients' memory recovery.

https://thejns.org/doi/abs/10.3171/2021.1.JNS203959

KEYWORDS brain tumors; memory; default mode network; diffusion MRI; neurosurgery; brain networks; oncology

ABBREVIATIONS DMN = default mode network; DTI = diffusion tensor imaging; FA = fractional anisotropy; F_{val} = F (statistic) value derived from the LMM; LMM = linear mixed-effect model; MDT = multidisciplinary team; NODDI = neurite orientation dispersion and density imaging; OCS = Oxford Cognitive Screen; P_{fdr} = p value after false discovery rate correction.

SUBMITTED November 3, 2020. **ACCEPTED** January 25, 2021.

INCLUDE WHEN CITING Published online August 6, 2021; DOI: 10.3171/2021.1.JNS203959.

* R.R.G. and J.S. contributed equally to this work.

Every year more than 300,000 people worldwide face the diagnosis of a brain tumor. Patients who undergo resection rather than biopsy have a better overall survival, and extending the resection beyond the abnormality seen on MRI may further improve prognosis. However, the extent of resection is only a worthwhile prognostic factor in the management of the tumor if subsequent cognitive functioning can be maintained. Cognitive function, despite being recognized as a fundamental outcome measure of treatment success, remains one of the most unpredictable aspects of patients' prognosis. As a result of their tumors, a significant proportion of patients develop cognitive deficits ranging from 29% in patients with nonirradiated low-grade glioma, to approximately 90% in patients following chemoradiotherapy for metastases.[1] Among the wide range of acquired cognitive deficits, memory disabilities represent a major challenge for preserving patients' quality of life, including job preservation.[2] Working,[3] verbal,[4] and nonverbal[5] memory deficits have been extensively reported in patients with brain tumors. Pharmacological interventions improve memory recovery,[6] which has been validated in animal models.[7] Unfortunately, the impact of surgery on cognitive outcome and memory has traditionally been underappreciated, potentially due to the complex distributed networks involved in normal memory function, and the limited understanding of how focal lesions interact with these networks.[8]

Typical MRI sequences used for clinical evaluation are limited by low biological specificity that constrains their capability to differentiate tumor types and infiltration as well as determine macromolecular and histological compositions. For example, although gadolinium contrast enhancement is currently used with MRI as a marker of anaplastic transformation of diffuse lower-grade gliomas, up to one-third of high-grade gliomas are nonenhancing.[9] Alternatively, diffusion MRI sequences probe the random (Brownian) motion of extracellular water and the restricted diffusion of intracellular water to determine brain tissue microstructure and orientation. Diffusion MRI protocols have been exploited for estimating tumor infiltration, grading, heterogeneity, progression, and patient survival,[10] suggesting that the incorporation of these MRI protocols into the clinical routine may also be useful in reducing treatment-induced neurocognitive dysfunction in brain tumors. Notwithstanding, most previous brain tumor studies have used diffusion models under the assumption of gaussian diffusion processes.

In contrast, the neurite orientation dispersion and density imaging (NODDI) technique uses varying diffusion gradient strengths to provide more specific measurements of neurite morphology—such as density and orientation dispersion—that cannot be derived from traditional diffusion MRI.[11] NODDI models the diffusion signal by separating the brain tissue into three compartments: intraneurite water, extraneurite water, and CSF. The volume fraction of the intraneurite compartment has been established as a marker of neurite density that has been validated using histochemical analysis in mouse models[12] and has shown sensitivity to neurotypical aging,[13] and has also been used for detecting axonal degeneration in neurological (such as Alzheimer disease[14] and multiple sclerosis[15]) and psychiatric conditions.[16] Caverzasi et al. (2016) showed that even for tumor lesions that appear to be homogeneous on corresponding FLAIR images, NODDI has the potential to differentiate infiltrative tumor components.[17] Additionally, NODDI has been demonstrated to be an accurate predictor of glioma grade.[18] Despite these promising findings, no study has yet used NODDI to evaluate the impact of tumors and their treatment on cognition, including memory.

A major challenge when predicting the consequences of surgery and chemoradiotherapy is that higher-order cognitive functions such as memory are subserved by communication across spatially extended neural circuits that will require whole-brain analysis approaches. Large-scale brain networks offer a holistic framework for analyzing the brain as a circuit of interacting components that are critically related to cognition.[19] In neurooncology, markers derived from brain network approaches have been demonstrated to be sensitive to the presence of low-grade gliomas, plasticity differences between low- and high-grade gliomas, and surgically induced alterations.[20] Consequently, the use of brain network data to explore the potential for memory disruption induced by brain tumors and their treatment could be of major clinical relevance.

In this longitudinal study we prospectively investigated a cohort of patients with diffuse glioma and also asked whether MRI could be used to predict cognitive recovery postoperatively and during follow-up. Specifically, we wished to test the effect of tumors both locally and globally on the brain, in terms of their structural and functional network effects. We hypothesized that treatment-induced memory deficits are caused by disruption of brain networks that have been previously identified as fundamental for memory, and that this is mediated by global effects on normal brain microstructure.

Methods

Patient Sample

This study is a single-center prospective cohort design approved by the Cambridge Central Research Ethics Committee. Patients deemed to have typical appearances of a diffuse glioma were identified at adult neurooncology multidisciplinary team (MDT) meetings at Addenbrooke's Hospital (Cambridge, UK), and a consultant neurosurgeon directly involved in the study identified potential patients based on the outcome of the MDT discussion. All patients gave written informed consent. Inclusion criteria included the following: 1) participant was willing and able to give informed consent for participation in the study; 2) imaging was evaluated by the MDT and judged to have typical appearances of a diffuse glioma; 3) Stealth MRI was obtained (routine neuronavigation MRI scan performed prior to surgery); 4) WHO performance status 0 or 1; 5) age between 18 and 80 years; 6) tumor located in or near eloquent areas of the brain thought to be important for speech and executive functions; and 7) patient was undergoing awake resection of a diffuse glioma. This last inclusion criterion was adopted to collect additional intraoperative electrocorticography data that will be re-

TABLE 1. Demographic and pathological information in 17 patients with diffuse nonenhancing glioma

Case No.	Age (yrs)	Gender	Dom Hand	Presentation	Hemi	Location	Histology (WHO grade)	Molecular Signature	Lesion Vol Pre/Post (cm^3)*	Neurite Density†		Treatment
										Preop	Postop	
1	41	F	Lt	Seizures	Lt	Frontal	Oligo (II)	*IDH* mutated; *1p19q* lost; *ATRX* retained	166.8/94.5	0.0666	Missing	Chemo-RT
2	32	M	Rt	Seizures	Rt	Insula	Astro (II)	*IDH* WT; *1p19q* lost; *ATRX* lost	83.2/47.8	0.074	0.0758	Chemo-RT
3	26	M	Rt	Seizures	Lt	Temporal/ Insula	GBM (IV)	*IDH* mutated; *1p19q* lost; *ATRX* lost	59.0/30.1	0.0677	0.0719	Chemo-RT
4	49	F	Rt	Incidental	Rt	Insula	Oligo (II)	*IDH* mutated; *1p19q* lost; *ATRX* retained	31.5/37.5	0.0765	0.0718	Observation
5	55	F	Rt	Recurrence	Lt	Frontal/SFG/ frontal pole	Oligo (II)	*IDH* mutated; *1p19q* lost; *ATRX* retained	21.1/43.4	0.0636	0.0631	Observation
6	22	F	Lt	Seizures	Rt	Frontal/IFG	Ganglio-glioma (I)	*IDH* WT	4.4/7.5	0.0659	0.0669	Observation
7	29	M	Rt	Seizures	Rt	Frontal/SFG & MFG	Astro (III)	*IDH* mutated; *1p19q* lost; *ATRX* lost	31.8/70.0	0.0897	0.0843	Chemo-RT
8	29	M	Rt	Seizures	Rt	Frontal/MFG	Astro (III)	*IDH* mutated; *1p19q* lost; *ATRX* lost	22.6/34.2	0.0725	0.0717	Chemo-RT
9	50	M	Lt	Seizures	Lt	Temporal/ ITG	GBM (IV)	*IDH* WT; *1p19q* lost; *ATRX* retained	15.6/15.7	0.081	0.0816	Chemo-RT
10	38	F	Rt	Seizures	Rt	Frontal/MFG	Oligo (II)	*IDH* mutated; *1p19q* lost; *ATRX* retained	34.7/54.9	0.0819	0.0826	Chemo-RT
11	29	M	Rt	Seizures	Lt	Frontal/SFG/ frontal pole	Astro (II)	*IDH* mutated; *1p19q* lost; *ATRX* lost	52.1/116.9	0.0694	0.0686	Observation
12	33	F	Rt	Headaches	Lt	Temporal/ MTG	Astro (III)	*IDH* mutated; *1p19q* lost; *ATRX* lost	87.0/84.8	0.0694	0.0693	Chemo-RT
13	27	F	Rt	Seizures	Lt	STG	Ganglio-glioma (I)	*IDH* WT; *1p19q* lost; *ATRX* lost	7.6/8.5	0.0854	Missing	Observation
14	56	F	Rt	Seizures	Lt	STG	Astro (II)	*IDH* mutated; *1p19q* lost; *ATRX* lost	37.4/19.2	0.0653	0.0638	Chemo-RT
15	32	M	Rt	Seizures	Lt	STG	Astro (III)	*IDH* mutated; *1p19q* lost; *ATRX* lost	18.0/30.3	0.0823	0.0776	Chemo-RT
16	27	M	Rt	Seizures	Lt	SFG/SMA & precentral	GBM (IV)	*IDH* WT; *1p19q* lost; *ATRX* retained	73.6/43.7	0.0629	0.0719	Chemo-RT
17	30	M	Rt	Seizures	Lt	IFG	Astro (III)	*IDH* mutated; *1p19q* lost; *ATRX* lost	26.2/17.4	0.081	0.0816	Chemo-RT

Astro = astrocytoma; chemo-RT = chemoradiotherapy; Dom = dominant; GBM = glioblastoma multiforme; Hemi = hemisphere; IFG = inferior frontal gyrus; ITG = inferior temporal gyrus; MFG = middle frontal gyrus; MTG = middle temporal gyrus; oligo = oligodendroglioma; SFG = superior frontal gyrus; SMA = supplementary motor area; STG = superior temporal gyrus; WT = wild-type.

* Total volume occupied by the tumor (pre) and total amount of damaged tissue (post) according to the lesion mask manually drawn on the MPRAGE image and refined with the Unified Segmentation with Lesion toolbox.

† Preoperative and postoperative neurite density was calculated as the average neurite density for the whole brain of each individual.

ported separately.[21] Participants were excluded if any of the following applied: 1) concomitant anticancer therapy; 2) concomitant treatment with steroids; 3) history of previous malignancy (except for adequately treated basal and squamous cell carcinoma or carcinoma in situ of the skin) within 5 years; and 4) previous severe head injury.

We recruited 17 patients ages 22–56 years (8 women). Final histological diagnoses revealed different grades of glioma: WHO I, n = 2; WHO II, n = 7; WHO III, n = 5; and WHO IV, n = 3. Resection was complete (no residual FLAIR signal) in 9 patients, whereas 8 patients had partial resection. Adjuvant chemoradiotherapy was performed in 12 patients. Each patient was scanned up to 4 times: before surgery (preoperatively); within 72 hours after surgery (postoperatively); and at 3 and 12 months after surgery (month 3 and month 12). See Table 1 for demographic details of participants.

MRI and NODDI Data Acquisition and Preprocessing

MRI data were acquired using a Siemens Magnetom Prisma-fit 3-T MRI scanner and 16-channel receive-only head coil (Siemens AG). A T1-weighted MRI MPRAGE

sequence was acquired using the following parameters: TR = 2300 msec, TE = 2.98 msec, flip angle = 9°, 1-mm^3 resolution, field of view = 256 × 240 mm, 192 contiguous slices, and acquisition time of 9 minutes and 14 seconds. During the same scanning session, we used a recently developed MRI multishell diffusion technique, NODDI with 30 directions (b-value = 800 mm/sec), 60 directions (b-value = 2000 mm/sec), and 10 unweighted B0 images. Other acquisition parameters were as follows: TR = 8200 msec, TE = 95 msec, 2.5-mm^3 voxel resolution, 60 slices, field of view = 240 × 240 mm, and acquisition time of 15 minutes and 19 seconds. The NODDI Matlab Toolbox (http://mig.cs.ucl.ac.uk/index.php?n=Tutorial.NODDImatlab) was used to quantify the microstructural complexity of dendrites and axons in vivo.[11] Compared with traditional diffusion tensor imaging (DTI), this multicompartment tissue model disentangles two key contributing factors to fractional anisotropy (FA): the gaussian contribution from water molecules located in the extracellular space (defined as the space around neurites), and the restricted non-gaussian diffusion that takes place in the intracellular space that is bounded by axonal and dendritic membranes. The apparent intracellular volume fraction that represents the fraction of dendrites and axons was used here as a measurement of neurite density.

Lesion Masking and Image Transformation to Standard Space

Images were corrected for B0 field inhomogeneity, Gibbs artifacts, and eddy-current distortions using MRtrix v3 (https://www.mrtrix.org/) and FSL v5.0 (http://fsl.fmrib.ox.ac.uk). Scans were visually inspected by an experienced researcher (R.R.G.). Masks of the preoperative tumor and the lesion at follow-up (reflecting for example resected tissue, residual tumor, postsurgical edema, or gliosis) masks were created using a semiautomated procedure. An experienced neurosurgeon (M.G.H.) initially did a manual delineation for each participant on the preoperative T1 image slices that included the tumor, and also did the resection site on the follow-up T1 images. The resulting masks were refined by the Unified Segmentation with Lesion toolbox (https://github.com/CyclotronResearchCentre/USwithLesion), which uses tissue probability maps to create a posterior tumor/lesion probability map. Interregional distances to the tumor boundary as defined in the tumor mask were estimated as the geodesic distance of the shortest path constrained by the white matter.

For each scan, the first B0 image of the diffusion-sensitive sequence was linearly coregistered to the T1 image by using advanced normalization tools (ANTs; http://stnava.github.io/ANTs/). The resulting inverse transformation was used to map the neurite density map into the T1 image space. Each T1 image was nonlinearly coregistered to standard space by using symmetric normalization (ANTsSyN), but excluding the tumor/lesion mask from the nonlinear step of the wrapping to avoid distorting the spatial distribution of the tumor/lesion. The resulting transformation was additionally used to map the lesion mask and the neurite density map from T1 image space to standard template space. The ICBM 2009a symmetric brain, an unbiased nonlinear average of the MNI152, was used here as a standard template for normalization of neurite density by dividing the values of the affected hemisphere by the values of the contralateral hemisphere.

Networks Atlas Based on Normative Data

We additionally used the map of large-scale networks defined in Yeo et al. (2011).[22] This atlas was created by clustering functionally coupled regions in 1000 young, healthy adults. Regions delimited on the 7-network liberal version of the Yeo atlas were used as regions of interest for calculating tumor overlap and neurite density (Fig. 1, upper row). The visual network was not included in the analyses because none of the patients presented with a tumor in the occipital lobe. The limbic network was also excluded from further analyses due to its poor signal-to-noise ratio and lack of reproducibility.[23]

Tumor Overlapping and Neurite Density Estimation

Because location of the tumor varied across patients, we calculated the tumor overlap index for each network and participant. This index was calculated as the amount of regional volume (in mm^3) that spatially overlapped with the tumor (for preoperative assessments) or lesioned tissue (for postoperative and follow-up assessments) according to the tumor/lesion masks, after being transformed to standard space. The median neurite densities in each Yeo network were calculated for each participant. Only voxels of the network that were not overlapping with the tumor/lesion masks were included in the analysis, to reduce the impact of tumor volume on neurite density estimation. See Fig. 1 for an illustrative flowchart.

Cognitive Assessment

Immediately after each MRI scanning session, memory performance was evaluated using the Oxford Cognitive Screen (OCS)–bridge tablet-based tool (https://ocs-bridge.com/), which is specifically designed for the clinical setting. OCS-bridge is an app-based extension of the Birmingham Cognitive Screen and the OCS, two paper-and-pencil assessment tests that are widely used in health services in the UK and that have been translated into multiple languages.[24]

We performed 6 memory screening tasks that included the following: free verbal memory, overall verbal memory, episodic memory, orientation, forward digit span, and backward digit span. For each individual task a z-score value was computed by subtracting the mean and dividing by the standard deviation of task scores across participants. Tasks defined by an inverted scale in which high values represent low memory performance were flipped by multiplying the z-score by –1. Total memory score was calculated as the average z-score of all tasks. By subtracting the preoperative z-score from the z-score of each subsequent task, we defined the longitudinal trajectory of each assessment (Δ), where negative scores represent worse performance than before surgery (i.e., memory deficit) and positive scores are associated with increased performance compared with before surgery (i.e., memory improvement). We have recently demonstrated that memory

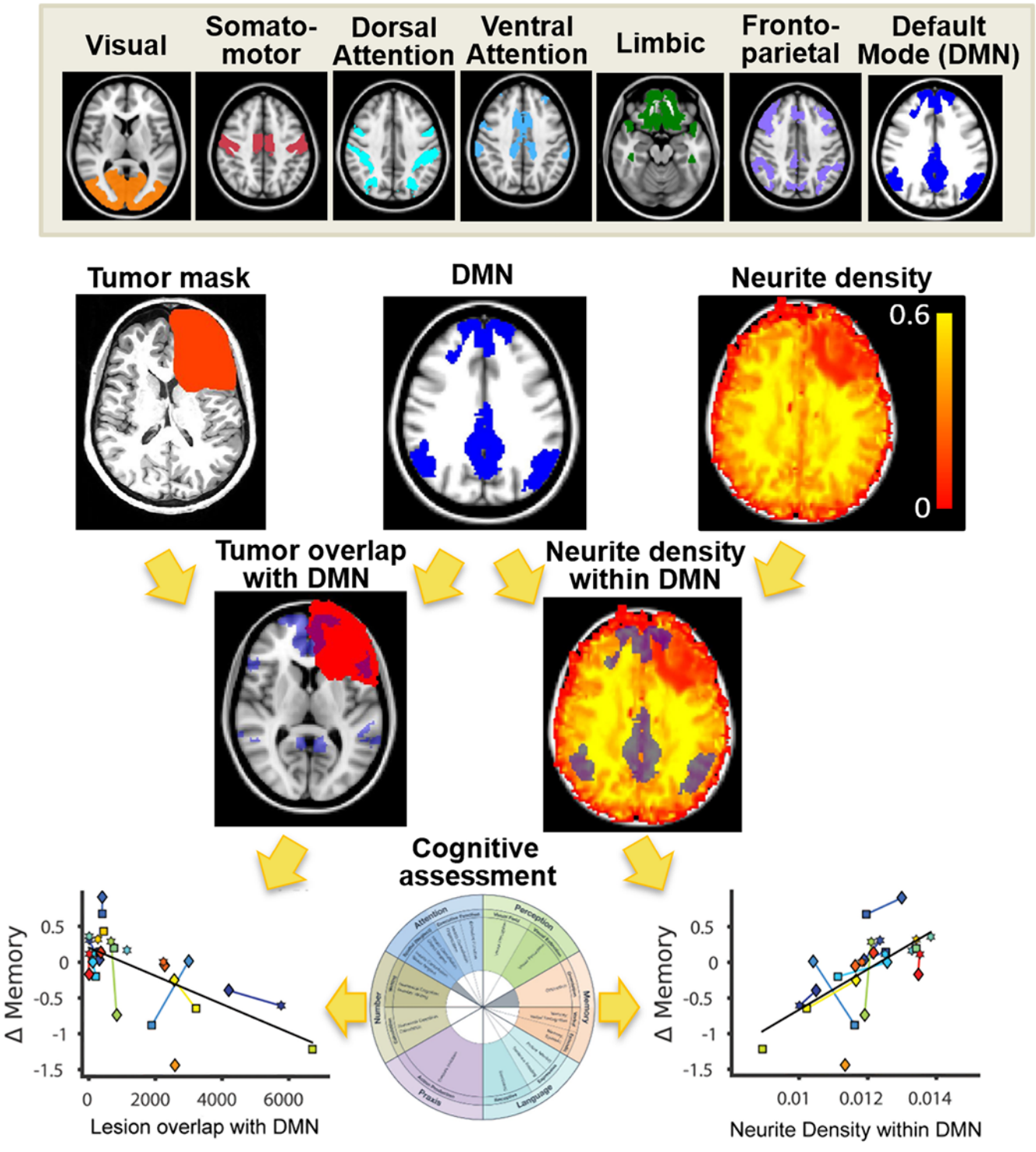

FIG. 1. Flowchart of pipeline analysis. After transforming lesion masks to standard space, tumor/lesion spatial overlap and neurite density were calculated for each Yeo network.[22] For each assessment (preoperative, postoperative, 3 months, and 12 months), lesion overlap and neurite density were compared with memory recovery. Figure is available in color online only.

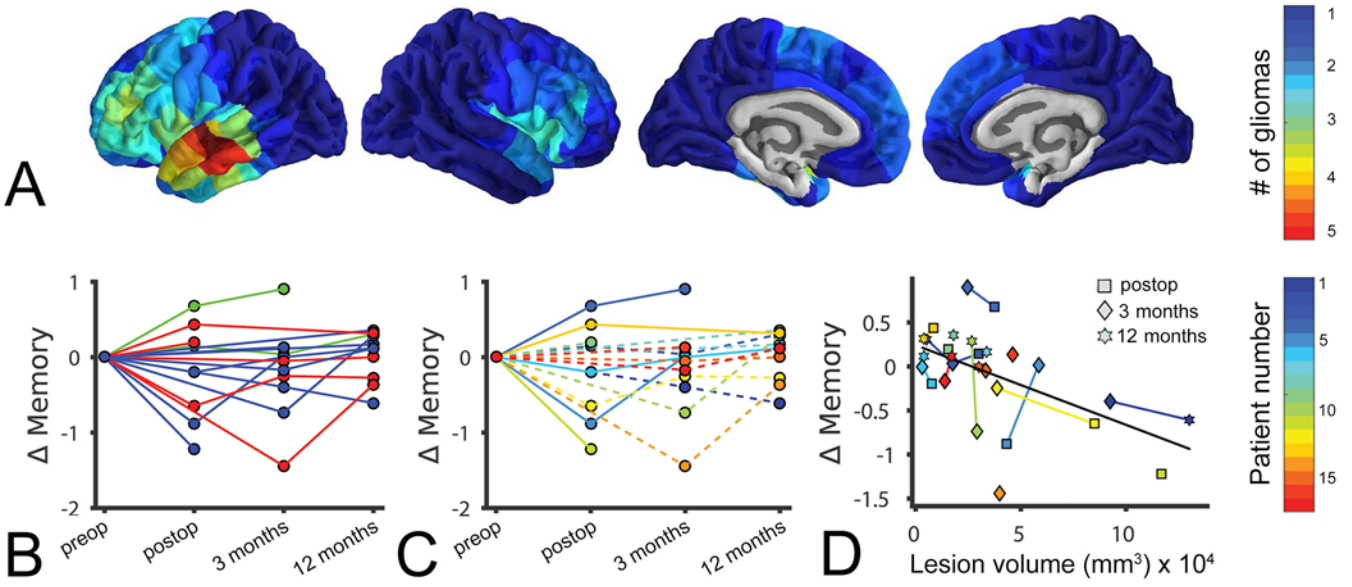

FIG. 2. Patients' memory recovery trajectories as a function of tumor location and type of treatment. **A:** Tumor location in the cohort. Color scale indicates the number of participants who had a tumor in a given cortical region. Cortical surface representations were plotted using BrainsForPublication v0.2.1 (https://doi.org/10.5281/zenodo.1069156). **B:** Memory recovery trajectories normalized to preoperative values colored according to tumor location (frontal, *blue*; temporal, *red*; insular, *green*). **C:** Recovery trajectories of patients receiving no further treatment beyond surgery (*solid lines*) and patients who also underwent chemoradiotherapy (*dashed lines*). **D:** Association between total lesion volume and memory recovery (postoperative, 3 months, and 12 months) across patients. Memory recovery was normalized to presurgical values. Each color represents an individual participant as presented in Table 1. Positive scores correspond with postsurgical memory recovery and negative scores with postsurgical deficits. Figure is available in color online only.

scores of these patients with brain tumors are consistent between OCS-bridge and a traditional 2- to 3-hour neuropsychological interview.[5]

Statistical Analysis

Associations between cognition and imaging markers were tested using linear mixed-effect models (LMMs) to account for the dependency of repeated measurements:

$$\Delta Memory = 1 + \beta_x \cdot X + \beta_{age} \cdot age + \beta_{gender} \cdot gender + \beta_{grade} \cdot grade + \beta_{treatment} \cdot treatment + \beta_{vol} \cdot vol + \beta_{ND} \cdot ND + (1 \mid subject),$$

where ΔMemory represents the total memory score normalized to preoperative performance, X is the predictor variable based on imaging data (i.e., tumor overlap or neurite density for a given network), and (1 |subject) represents the random intercept of the model. The model included as covariates the following: age, gender, grade (low- vs high-grade glioma), treatment (surgery alone vs surgery plus chemoradiotherapy), tumor volume, and total neurite density (ND; only for predictions based on neurite density). All statistical tests were corrected for multiple comparisons by using the Benjamini-Hochberg false discovery rate (fdr; < 0.05).

Missing data in limited sample size scenarios increase the chances of reporting false negatives. To partially address this issue, the main analyses were validated in an imputed data set constructed from deriving missing imaging and cognitive assessments by using a principal component analysis–based tool for data inference (Missing Data Imputation toolbox, trimmed scores regression algorithm, 5000 iterations, tolerance < 10^{-10}).[25]

Results

Memory Recovery Trajectories

Tumors were located on frontal (5 left hemisphere and 4 right hemisphere), temporal (6 left hemisphere), and insular (2 right hemisphere) lobes (Fig. 2A, Table 1). OCS-bridge cognitive assessment was completed by 17 patients before surgery, 8 after surgery, 11 after 3 months, and 11 after 12 months (47 in total). Seven patients could not tolerate postoperative screening and the remaining missing assessments could not be collected due to logistic and technical reasons (14 of 69). Years of education showed no correlation with preoperative memory performance ($R^2 = 0.03$, $p = 0.63$) or with memory recovery ($R^2 = 0.02$, $p = 0.50$). Resection and radiation treatment had an impact on memory in most participants. Memory recovery after surgery (ΔMemory) showed a variety of trajectories, including progressive impairment, impairment followed by recovery, no change, and improvement after surgery and during recovery.

No Impact of Tumor Location or Volume on Memory Recovery

Follow-up recovery trajectories were not associated with either the tumor location based on traditional lobe

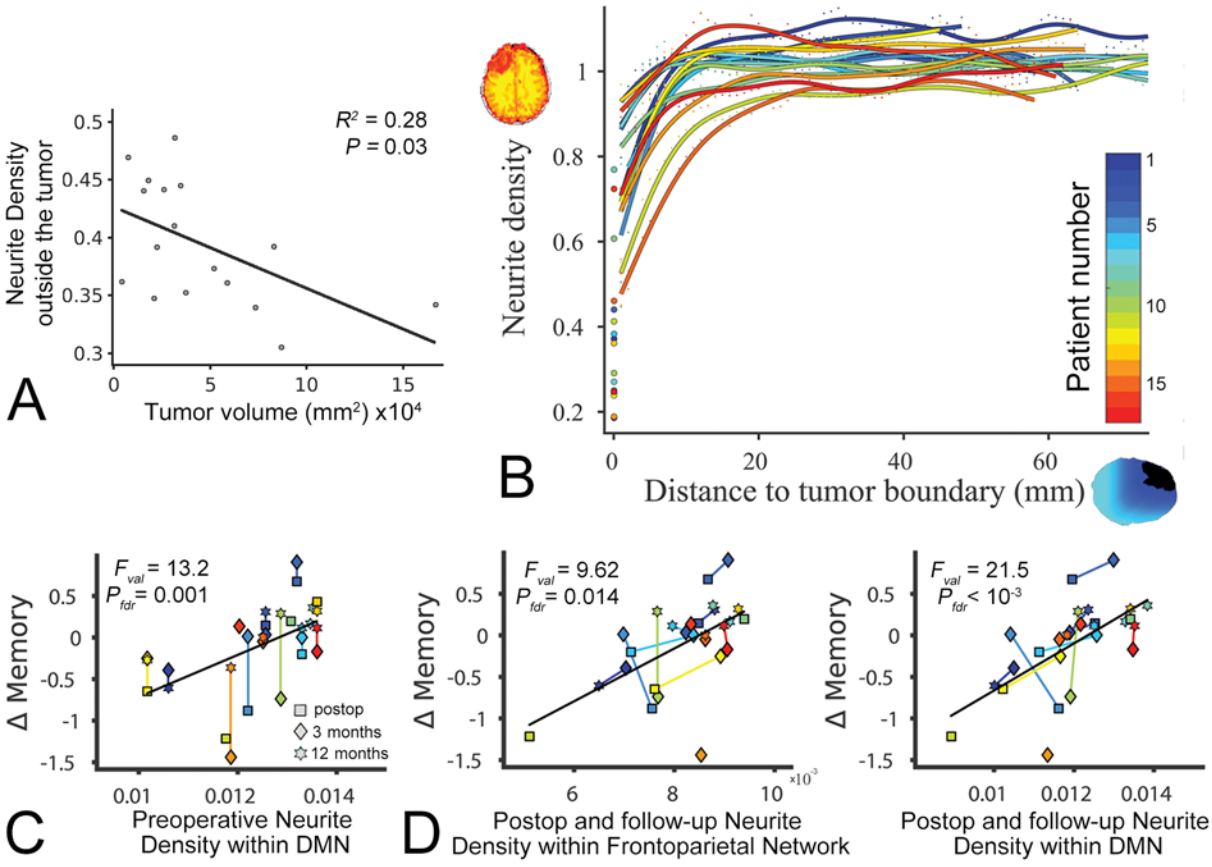

FIG. 3. Impact of tumor and tumor treatment in neurite density and memory recovery. **A:** Association between total tumor volume and neurite density outside of the tumor. **B:** Neurite density as a function of distance to the tumor boundary. Values are normalized to the contralateral hemisphere (i.e., values < 1 represent regions with reduced neurite density). Zero distance (x = 0 mm) corresponds to average neurite density values within each tumor. Each color represents an individual participant. Due to high-dimensional data, error bars are too small to be displayed. **C:** Memory recovery (postoperative, 3 months, and 12 months) as a function of preoperative neurite density within the DMN. For a given participant, the same neurite density (preoperative) value was used in all assessments, resulting in vertical lines between them. **D:** Memory recovery as a function of postoperative and follow-up neurite density within the frontoparietal network and DMN. Neurite density corresponds with the median density within the white matter of each network, excluding lesioned regions. Colors illustrate each participant, with lines connecting them. Figure is available in color online only.

classification (LMM, F [statistic] value [F_{val}] = 0.05, p = 0.11; Fig. 2B) or the type of treatment received by patients (i.e., surgery alone or surgery with adjuvant chemoradiotherapy; LMM, $F_{val} < 10^{-3}$, p = 0.98; Fig. 2C). The influence of the tumor and its treatment on recovery was initially evaluated by comparing the total lesion volume with changes in memory. Memory recovery was not correlated with either the tumor volume before surgery (Spearman's ρ = −0.27, p = 0.40) or lesion volume during recovery (LMM, F_{val} = 6.78, p = 0.097; Fig. 2D).

Peritumoral Neurite Density Within Brain Networks Is Associated With Memory Recovery

The impact of tumors and their treatment on brain structure was explored using a neurite density marker derived from diffusion-weighted imaging based on NODDI. Neurite density showed no correlation with age (R^2 = 0.02, p = 0.57), years of education (R^2 = 0.016, p = 0.62), preoperative memory performance (R^2 = 0.002, p = 0.87), or memory recovery (R^2 = 0.13, p = 0.06), but was significantly different between networks in the hemisphere contralateral to the tumor (F_{val} = 42.56, p < 10^{-18}; Fig. S1). We found that average whole-brain neurite density outside the tumor was negatively associated with tumor volume (R^2 = 0.28, p = 0.029; Fig. 3A), suggesting that tumors may mediate global effects on brain structural integrity. In support of this hypothesis, we found a distance effect on neurite density as a function of distance to the tumor boundary. Peritumoral regions located between 0 and 20 mm outward from the tumor boundary had up to half of the neurite density compared to contralateral regions (Fig. 3B), suggesting an extended tumor and brain structural integrity interaction. Preoperative neurite density within the default mode network (DMN) in both hemispheres (i.e., not normalized) was positively correlated with memory performance during recovery, suggesting that neurite density has an initial protective effect on outcome (F_{val} = 13.2, p value after false discovery rate correction [P_{fdr}] = 0.001;

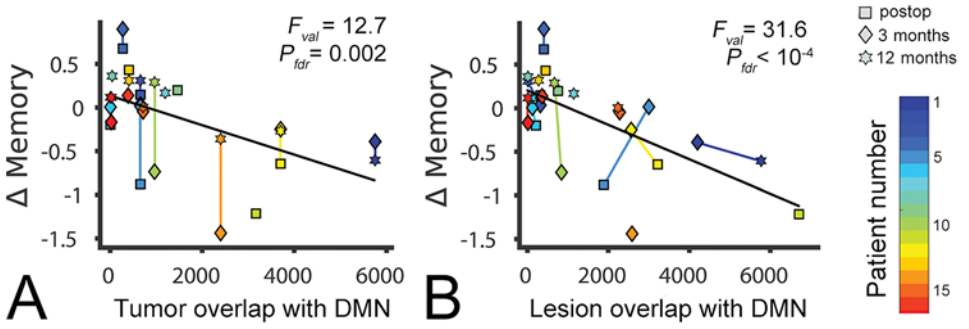

FIG. 4. A: Memory recovery as a function of tumor overlap with DMN. For a given participant, the (preoperative) tumor overlap value was used in all assessments, resulting in vertical lines between them. **B:** Memory recovery as a function of (follow-up) lesion overlap with DMN. Overlap values were defined as the number of voxels (equivalent to mm^3) of the tumor mask that overlapped with each network. Lines link assessments of the same participant. Figure is available in color online only.

Fig. 3C). Moreover, neurite density during recovery was also associated with memory performance. When postoperative and follow-up neurite density values were considered, memory scores were correlated with neurite density within the frontoparietal network (F_{val} = 9.62, P_{fdr} = 0.01) and DMN (F_{val} = 21.5, $P_{fdr} < 10^{-3}$) (Fig. 3D). Neither preoperative nor follow-up neurite density with any of the remaining networks was associated with memory recovery (all $P_{fdr} > 0.05$; Table S1). All associations were tested using LMM after regressing out age, gender, tumor grade, total lesion volume, type of treatment, and total neurite density effects. Results shown in Fig. 3C and D were validated using an imputed data set in which missing assessments were inferred from the available data (Fig. S2).

Tumor Overlap With the DMN Is Associated With Memory Recovery

Preoperative tumor overlap with the DMN was negatively correlated with memory recovery (F_{val} = 12.7, P_{fdr} = 0.002; Fig. 4A). When follow-up imaging data were included in the analyses (postoperative, 3 months, and 12 months), we also found a significant association between lesion overlapping with the DMN and memory performance (F_{val} = 31.6, $P_{fdr} < 10^{-4}$; Fig. 4B). Neither (preoperative) tumor nor (follow-up) lesion overlapping with any of the remaining networks was associated with memory recovery (all $P_{fdr} > 0.05$; Table S1). All associations were tested using LMM after regressing out age, gender, tumor grade, type of treatment, and total lesion volume effects. Results were validated using an imputation for missing data (Fig. S2).

Discussion

In this study we combined structural and NODDI diffusion MRI with normative brain network data from healthy participants and with whole-brain analyses to determine whether memory recovery trajectories are affected by the impact that the tumor and its treatment have on specific circuits. Overall, our results suggest that the effect of a tumor on the brain and its consequences in memory depends on interactions with the DMN at both global levels.

Acquiring high-quality longitudinal memory outcome data required a nuanced study design. Using a tablet-based cognitive assessment app afforded specific advantages, such as avoiding reliance on having a trained neuropsychologist available (with associated time and financial costs), more easily facilitating follow-up screening, and collecting specific data, such as accurate reaction times and interactive visuospatial paradigms, that are difficult to acquire using traditional clinical interviews and tests. We observed a variety of memory recovery trajectories after surgery and during subsequent treatment that included no change, postsurgical deterioration and then improvement, and postsurgical improvement and then deterioration. Although the mechanisms behind cognitive improvement after major surgery are not understood, these findings are not without precedent.[26] Nevertheless, given that pre- and postoperative assessments were performed in a relatively short period of time, we cannot discard the possibility of practice and learning effects on the tasks.

Tumor location is one of the most relevant features to be considered when estimating the cognitive risks of resection. In our cohort, gliomas were mainly located in frontal, temporal, and insular cortices on the left hemisphere. The higher prevalence of left-hemisphere tumors occurred because this study only included patients undergoing awake brain surgery. On the other hand, the higher prevalence of frontal, temporal, and insular tumors is consistent with previous studies showing that low- and high-grade gliomas are relatively scarce in primary cortices and occipital lobes.[27] Although several developmental, cytomyeloarchitectonic, neurochemical, metabolic, and functional reasons have been proposed, the mechanisms behind the preferential location of gliomas in frontal, temporal, and insular cortices are still an ongoing debate.[28] The presence of gliomas in secondary and association cortices that have been traditionally related to cognitive processing[29] may be an important factor to understand cognitive deficits induced by the tumor and its treatment.

Beyond the impact that age, gender, tumor grade, tumor volume, and type of treatment have on recovery, we hypothesized that memory functioning was associated with treatment-related interactions with brain networks that have been previously identified as fundamental for cognition and memory. In support of this hypothesis, we found significant associations between memory recovery

and lesion overlap with the DMN. The DMN constitutes a set of regions that are active during passive rest, and it is considered the neuronal correlate of internally generated, self-referential cognition. Accordingly, a large body of literature has accumulated evidence about the role of the DMN in memory functioning, including semantic,[30] episodic,[31] autobiographical,[32] and working memory.[33] Damage to the DMN has been associated with memory deficits in patients with brain lesions[32] and traumatic brain injury.[34] To the best of our knowledge, there are no studies linking DMN disruption with memory recovery in patients with brain tumors to date, but decreases of functional connectivity in this network have been extensively reported in the literature. DMN functional connectivity is reduced in patients with glioma when compared with controls in both the hemisphere ipsilateral and the one contralateral to the tumor, which is particularly prominent for tumors located on the left side of the brain.[35]

Neurite density derived from NODDI has been previously associated with age[36,37] and gender.[38] However, to the best of our knowledge there is no study formally exploring associations between neurite density and years of education or education level. Not surprisingly, we found a consistent neurite density decrease within the tumor. Given that neurite densities derived from NODDI and FA are strongly correlated,[11] our results align with previous evidence found from DTI studies showing that glioblastomas have reduced FA compared with the rest of the brain.[39] For its part, NODDI has shown higher sensitivity for glioma grade differentiation than have other diffusion sequences.[40] Zhao et al. (2018) recently reported that NODDI in combination with patient age can predict glioma grade with a sensitivity and specificity of 92% and 89%, respectively.[18] Despite these promising findings, the potential of NODDI as a predictor of patient cognitive recovery has not yet been explored in the literature.

Despite peritumoral regions being identified on T1 images as unaffected by the experienced neurosurgeon who delineated the mask, and by the semiautomatic segmentation procedure, these regions had decreased neurite density compared with the contralateral hemisphere. Long-distance tumor effects have been observed with regard to functional connectivity and functional complexity.[41] Disrupted white matter integrity has been reported in DTI studies that show decreased FA in peritumoral regions[42] and white matter tracts.[43] Extratumoral pre- and postoperative neurite density within the frontoparietal network and DMN was a protective factor in memory recovery that may be mediated by the prominent role of these networks in this cognitive domain. From the connectomic perspective, the cognitive performance of patients with brain tumors has been associated with hub-related structural connectivity within the DMN and frontoparietal network in hemispheres contralateral to the tumor.[44] By using connectomic metrics derived from both DTI and fMRI, Liu et al. (2016) achieved a 75% accuracy when predicting survival of patients with high-grade glioma.[45] However, further research is needed to better understand the mechanisms by which low- and high-grade glioma and treatment disruption mediate memory and, more generally, cognitive recovery.

Limitations

Brain tumors have a unique blood oxygen level–dependent fMRI signal compared with normal brain tissue.[46,47] For this reason, correlation-based time-series analysis, such as seed-based or independent component analysis, is problematic unless tumor tissue is excluded from the analysis. In the present study, including tumoral regions would have impeded the estimation of its overlap with each resting-state network. Consequently, brain networks were defined using normative data from healthy individuals.[22] However, by using brain network templates in standard space, we neglect the potential spatial shift of brain functioning. Thus, our results should be interpreted as the potential of the tumor to disrupt the corresponding healthy network, not the actual tumor/lesion overlap with each participant's network.

LMMs can accommodate missing data, prevent false-positive associations due to population structure, and increase power by applying a structure-specific correction. However, 17 patients still represent a limited sample size for a heterogeneous condition. For this reason, it is possible that some of the reported nonsignificant associations were type II errors. Moreover, treatment heterogeneity across patients also limits the generalizability of the results. Because treatment was decided solely on clinical criteria, 5 patients had only a surgical intervention, whereas 12 additionally had different chemoradiotherapy regimens. Chemoradiotherapy has a dose-dependent effect on white matter structural integrity that has been associated with poor cognitive performance.[48] Additionally, all of our patients had the preoperative imaging appearances of a diffuse glioma (for example, nonenhancing and without edema or mass effect), and subsequent pathological examination revealed a range of histological diagnoses, in keeping with previous studies demonstrating the diagnostic limitations of standard MRI sequences. Although the LMMs considered here regressed out the effect of age, gender, tumor grade, tumor volume, and treatment, the individual contribution of these factors cannot be untangled here due to the limited sample size.

Conclusions

Our findings highlight the fact that memory recovery is not associated with either the type of treatment, tumor volume, or the tumor location based on traditional lobes. Interestingly, neurite density is decreased beyond the tumor boundary, and high values within frontoparietal network and DMN are associated with better memory recovery. On the other hand, tumor and lesion overlapping with DMN have a negative impact on memory. Taken together, these results reveal the potential of combining brain network analyses, normative connectomes, and advanced MRI sequences to better understand and predict the impact of brain tumors and their treatment on patients' cognitive outcomes.

Acknowledgments

We thank all patients for generous involvement in the study. We also thank Luca Villa, Jessica Ingham, and Alexa Mcdonald for their contribution to the study. This research was supported by The Brain Tumour Charity, the Guarantors of Brain, and

the NIHR Cambridge Biomedical Research Centre (BRC-1215-20014).

References

1. Meyers CA, Smith JA, Bezjak A, et al. Neurocognitive function and progression in patients with brain metastases treated with whole-brain radiation and motexafin gadolinium: results of a randomized phase III trial. *J Clin Oncol*. 2004;22(1):157–165.
2. Rusbridge SL, Walmsley NC, Griffiths SB, et al. Predicting outcomes of vocational rehabilitation in patients with brain tumours. *Psychooncology*. 2013;22(8):1907–1911.
3. Teixidor P, Gatignol P, Leroy M, et al. Assessment of verbal working memory before and after surgery for low-grade glioma. *J Neurooncol*. 2007;81(3):305–313.
4. de Groot M, Douw L, Sizoo EM, et al. Levetiracetam improves verbal memory in high-grade glioma patients. *Neuro Oncol*. 2013;15(2):216–223.
5. Owen M, Romero-Garcia R, McDonald A, et al. Assessment of neuropsychological function during early treatment of diffuse glioma. *medRxiv*. Preprint posted online June 5, 2020. doi:10.1101/2020.06.03.20119255
6. Brown PD, Pugh S, Laack NN, et al. Memantine for the prevention of cognitive dysfunction in patients receiving whole-brain radiotherapy: a randomized, double-blind, placebo-controlled trial. *Neuro Oncol*. 2013;15(10):1429–1437.
7. Schültke E, Juurlink BHJ, Ataelmannan K, et al. Memory and survival after microbeam radiation therapy. *Eur J Radiol*. 2008;68(3)(suppl):S142–S146.
8. Sagberg LM, Drewes C, Jakola AS, Solheim O. Accuracy of operating neurosurgeons' prediction of functional levels after intracranial tumor surgery. *J Neurosurg*. 2017;126(4):1173–1180.
9. Scott JN, Brasher PMA, Sevick RJ, et al. How often are nonenhancing supratentorial gliomas malignant? A population study. *Neurology*. 2002;59(6):947–949.
10. Villanueva-Meyer JE, Mabray MC, Cha S. Current clinical brain tumor imaging. *Neurosurgery*. 2017;81(3):397–415.
11. Zhang H, Schneider T, Wheeler-Kingshott CA, Alexander DC. NODDI: practical in vivo neurite orientation dispersion and density imaging of the human brain. *Neuroimage*. 2012;61(4):1000–1016.
12. Wang N, Zhang J, Cofer G, et al. Neurite orientation dispersion and density imaging of mouse brain microstructure. *Brain Struct Funct*. 2019;224(5):1797–1813.
13. Nazeri A, Chakravarty MM, Rotenberg DJ, et al. Functional consequences of neurite orientation dispersion and density in humans across the adult lifespan. *J Neurosci*. 2015;35(4):1753–1762.
14. Colgan N, Siow B, O'Callaghan JM, et al. Application of neurite orientation dispersion and density imaging (NODDI) to a tau pathology model of Alzheimer's disease. *Neuroimage*. 2016;125:739–744.
15. Grussu F, Schneider T, Tur C, et al. Neurite dispersion: a new marker of multiple sclerosis spinal cord pathology? *Ann Clin Transl Neurol*. 2017;4(9):663–679.
16. Rae CL, Davies G, Garfinkel SN, et al. Deficits in neurite density underlie white matter structure abnormalities in first-episode psychosis. *Biol Psychiatry*. 2017;82(10):716–725.
17. Caverzasi E, Papinutto N, Castellano A, et al. Neurite orientation dispersion and density imaging color maps to characterize brain diffusion in neurologic disorders. *J Neuroimaging*. 2016;26(5):494–498.
18. Zhao J, Li JB, Wang JY, et al. Quantitative analysis of neurite orientation dispersion and density imaging in grading gliomas and detecting *IDH-1* gene mutation status. *Neuroimage Clin*. 2018;19(4):174–181.
19. Bressler SL, Menon V. Large-scale brain networks in cognition: emerging methods and principles. *Trends Cogn Sci*. 2010;14(6):277–290.
20. Huang Q, Zhang R, Hu X, et al. Disturbed small-world networks and neurocognitive function in frontal lobe low-grade glioma patients. *PLoS One*. 2014;9(4):e94095.
21. Erez Y, Assem M, Coelho P, et al. Intraoperative mapping of executive function using electrocorticography for patients with low-grade gliomas. *Acta Neurochir (Wien)*. 2021;163(5):1299-1309.
22. Yeo BT, Krienen FM, Sepulcre J, et al. The organization of the human cerebral cortex estimated by intrinsic functional connectivity. *J Neurophysiol*. 2011;106(3):1125–1165.
23. Gordon EM, Laumann TO, Adeyemo B, et al. Generation and evaluation of a cortical area parcellation from resting-state correlations. *Cereb Cortex*. 2016;26(1):288–303.
24. Kong APH, Lam PHP, Ho DWL, et al. The Hong Kong version of the Oxford Cognitive Screen (HK-OCS): validation study for Cantonese-speaking chronic stroke survivors. *Neuropsychol Dev Cogn B Aging Neuropsychol Cogn*. 2016;23(5):530–548.
25. Folch-Fortuny A, Arteaga F, Ferrer A. Missing data imputation toolbox for MATLAB. *Chemometr Intell Lab Syst*. 2016;154(5):93–100.
26. Habets EJJ, Kloet A, Walchenbach R, et al. Tumour and surgery effects on cognitive functioning in high-grade glioma patients. *Acta Neurochir (Wien)*. 2014;156(8):1451–1459.
27. De Witt Hamer PC, Hendriks EJ, Mandonnet E, et al. Resection probability maps for quality assessment of glioma surgery without brain location bias. *PLoS One*. 2013;8(9):e73353.
28. Mandal AS, Romero-Garcia R, Hart MG, Suckling J. Genetic, cellular, and connectomic characterization of the brain regions commonly plagued by glioma. *Brain*. 2020;143(11):3294–3307.
29. Goldman-Rakic PS. Topography of cognition: parallel distributed networks in primate association cortex. *Annu Rev Neurosci*. 1988;11(1):137–156.
30. Wirth M, Jann K, Dierks T, et al. Semantic memory involvement in the default mode network: a functional neuroimaging study using independent component analysis. *Neuroimage*. 2011;54(4):3057–3066.
31. McCormick C, Quraan M, Cohn M, et al. Default mode network connectivity indicates episodic memory capacity in mesial temporal lobe epilepsy. *Epilepsia*. 2013;54(5):809–818.
32. Philippi CL, Tranel D, Duff M, Rudrauf D. Damage to the default mode network disrupts autobiographical memory retrieval. *Soc Cogn Affect Neurosci*. 2015;10(3):318–326.
33. Sambataro F, Murty VP, Callicott JH, et al. Age-related alterations in default mode network: impact on working memory performance. *Neurobiol Aging*. 2010;31(5):839–852.
34. Sours C, Zhuo J, Janowich J, et al. Default mode network interference in mild traumatic brain injury—a pilot resting state study. *Brain Res*. 2013;1537(11):201–215.
35. Ghumman S, Fortin D, Noel-Lamy M, et al. Exploratory study of the effect of brain tumors on the default mode network. *J Neurooncol*. 2016;128(3):437–444.
36. Merluzzi AP, Dean DC III, Adluru N, et al. Age-dependent differences in brain tissue microstructure assessed with neurite orientation dispersion and density imaging. *Neurobiol Aging*. 2016;43:79–88.
37. Chang YS, Owen JP, Pojman NJ, et al. White matter changes of neurite density and fiber orientation dispersion during human brain maturation. *PLoS One*. 2015;10(6):e0123656.
38. Kodiweera C, Alexander AL, Harezlak J, et al. Age effects and sex differences in human brain white matter of young to middle-aged adults: A DTI, NODDI, and q-space study. *Neuroimage*. 2016;128:180–192.
39. Sinha S, Bastin ME, Whittle IR, Wardlaw JM. Diffusion tensor MR imaging of high-grade cerebral gliomas. *AJNR Am J Neuroradiol*. 2002;23(4):520–527.

40. Vellmer S, Tonoyan AS, Suter D, et al. Validation of DWI pre-processing procedures for reliable differentiation between human brain gliomas. *Z Med Phys*. 2018;28(1):14–24.
41. Hart MG, Romero-Garcia R, Price SJ, Suckling J. Global effects of focal brain tumors on functional complexity and network robustness: a prospective cohort study. *Neurosurgery*. 2019;84(6):1201–1213.
42. Holly KS, Barker BJ, Murcia D, et al. High-grade gliomas exhibit higher peritumoral fractional anisotropy and lower mean diffusivity than intracranial metastases. *Front Surg*. 2017;4:18.
43. Miller P, Coope D, Thompson G, et al. Quantitative evaluation of white matter tract DTI parameter changes in gliomas using nonlinear registration. *Neuroimage*. 2012;60(4):2309–2315.
44. Douw L, Miller JJ, Steenwijk MD, et al. Altered structural hub connectivity and its clinical relevance in glioma. *bioRxiv*. Preprint posted online April 16, 2019. doi:10.1101/610618
45. Liu L, Zhang H, Rekik I, et al. Outcome prediction for patient with high-grade gliomas from brain functional and structural networks. In: Ourselin S, Joskowicz L, Sabuncu M, eds. *Medical Image Computing and Computer-Assisted Intervention—MICCAI 2016*. *Lecture Notes in Computer Science*. Vol 9901. Springer; 2016:26–34.
46. Feldman SC, Chu D, Schulder M, et al. The blood oxygen level-dependent functional MR imaging signal can be used to identify brain tumors and distinguish them from normal tissue. *AJNR Am J Neuroradiol*. 2009;30(2):389–395.
47. Huang H, Lu J, Wu J, et al. Tumor tissue detection using blood-oxygen-level-dependent functional MRI based on independent component analysis. *Sci Rep*. 2018;8(1):1223.
48. Deprez S, Amant F, Smeets A, et al. Longitudinal assessment of chemotherapy-induced structural changes in cerebral white matter and its correlation with impaired cognitive functioning. *J Clin Oncol*. 2012;30(3):274–281.

Disclosures

The authors report no conflict of interest concerning the materials or methods used in this study or the findings specified in this paper.

Author Contributions

Conception and design: Romero-Garcia, Suckling, Assem, Sinha, Coelho, Woodberry, Price, Burke, Santarius, Erez, Hart. Acquisition of data: Romero-Garcia, Suckling, Owen, Sinha, Coelho, Woodberry, Santarius, Erez, Hart. Analysis and interpretation of data: Romero-Garcia, Suckling, Owen, Assem, Price, Burke, Santarius, Erez, Hart. Drafting the article: Romero-Garcia, Suckling, Price, Santarius, Erez, Hart. Critically revising the article: all authors. Reviewed submitted version of manuscript: all authors. Approved the final version of the manuscript on behalf of all authors: Romero-Garcia. Statistical analysis: Romero-Garcia, Suckling, Owen, Hart. Administrative/technical/material support: Romero-Garcia, Suckling, Woodberry, Santarius, Hart. Study supervision: Romero-Garcia, Suckling, Price, Santarius, Erez, Hart.

Supplemental Information

Online-Only Content

Supplemental material is available with the online version of the article.

Figures S1 and S2 and Table S1. https://thejns.org/doi/suppl/10.3171/2021.1.JNS203959.

Preprint Server

An earlier version of this article can be found on a preprint server.
Preprint server name: medRxiv.
Preprint DOI: 10.1101/19008581.

Correspondence

Rafael Romero-Garcia: University of Cambridge, United Kingdom. rr480@cam.ac.uk.